Strain-induced switching between noncollinear and collinear spin configuration in magnetic Mn_5Ge_3 films

Yufang Xie,[1,4,*] Ye Yuan,[2,9] Magdalena Birowska,[3] Chenhui Zhang,[2] Lei Cao,[1] Mao Wang,[1] Joerg Grenzer,[1] Dominik Kriegner,[5,6] Petr Doležal,[7] Yu-Jia Zeng,[8] Xixiang Zhang,[2] Manfred Helm,[1,4] Shengqiang Zhou,[1] and Slawomir Prucnal[1,†]

[1]*Institute of Ion Beam Physics and Materials Research, Helmholtz-Zentrum Dresden-Rossendorf, Bautzner Landstrasse 400, D-01328 Dresden, Germany*
[2]*Physical Science and Engineering Division, King Abdullah University of Science and Technology, 23955–6900 Thuwal, Saudi Arabia*
[3]*Faculty of Physics, Institute of Theoretical Physics, University of Warsaw, Pasteura 5, PL-02093 Warsaw, Poland*
[4]*Technische Universität Dresden, D-01062 Dresden, Germany*
[5]*Institut für Festkörper- und Materialphysik and Würzburg-Dresden Cluster of Excellence ct.qmat, Technische Universität Dresden, D-01062 Dresden, Germany*
[6]*Institute of Physics, Czech Academy of Sciences, Cukrovarnická 10, 162 00 Praha 6, Czech Republic*
[7]*Charles University, Faculty of Mathematics and Physics, Department of Condensed Matter Physics, Ke Karlovu 5, 121 16 Prague 2, Czech Republic*
[8]*College of Physics and Optoelectronic Engineering, Shenzhen University, Shenzhen 518060, People's Republic of China*
[9]*Songshan Lake Materials Laboratory, Dongguan, Guangdong 523808, People's Republic of China*

(Received 17 June 2021; revised 22 July 2021; accepted 26 July 2021; published 9 August 2021)

We report the temperature-dependent magnetic and structural properties of epitaxial Mn_5Ge_3 thin films grown on Ge substrates. Utilizing density-functional theory (DFT) calculations and various experimental methods, we reveal mechanisms governing the switching between collinear and noncollinear spin configuration in Mn_5Ge_3. The Mn atoms in Mn_5Ge_3 occupy two distinct Wyckoff positions with fourfold (Mn_1) and sixfold (Mn_2) multiplicity. The DFT calculations reveal that below a critical distance of approximately 3.002 Å the coupling between Mn_2 atoms is antiferromagnetic (AFM) while ferromagnetic (FM) above that critical distance. The FM coupling between Mn_1 atoms is weakly affected by the strain. The observed noncollinear spin configuration is due to the coexistence of AFM and FM coupling at low temperatures. The findings give insight in developing strain-controlled spintronic devices.

DOI: 10.1103/PhysRevB.104.064416

I. INTRODUCTION

Spintronic offers lower power dissipation and processing capabilities much beyond the current complementary metal oxide semiconductor technology [1,2]. However, it is very challenging to find a ferromagnetic semiconductor material with high Curie temperature (T_C) and compatible with Si technology. Ferromagnetic Mn_5Ge_3 films fabricated by epitaxial solid-state reaction on Ge substrates exhibit a T_C of about 283 K [3], a considerable spin polarization [4,5], a sharp interface between the ferromagnetic layer and Ge substrates [6,7], all of which are essential to achieve efficient spin injection and manipulation within semiconductors prepared by already-existing silicon-based technologies. Furthermore, the T_C of Mn_5Ge_3 was shifted much above room temperature by applying strain engineering (∼320 K) [8], quantum confinement (∼400 K) [9], or codoping with carbon (∼430 K) [10,11]. The fundamental properties of Mn_5Ge_3, especially the magnetic structure, have been investigated in detail [12–14]. Mn_5Ge_3 possesses a hexagonal $D8_8$-type crystal structure with space group $P6_3/mcm$ whose unit cell contains 6 Ge and 10 Mn atoms. The Mn atoms occupy two different sublattices where Mn_1 is located at the Wyckoff 4d site and Mn_2 at the 6g site with $x = 0.2397$ [14]. In the relaxed unit cell, the magnetic moment of Mn_1 is 1.96 μ_B/Mn and that of Mn_2 is 3.23 μ_B/Mn [14]. The magnetic moment direction of Mn_1 and Mn_2 atoms has been demonstrated to be parallel to the c axis of the hexagonal structure from 77 K to T_C. The distinguished magnetic coupling between two different sublattices leads to an anisotropic exchange and complex magnetic ordering in different temperature regimes.

Ab initio pseudopotential calculations have demonstrated that Mn_5Ge_3 has two competing phases with collinear and noncollinear spin configurations [15]. The interaction (J_1) between the nearest neighbors Mn_1-Mn_1 is ferromagnetic and weakly depends on the distance (d_1) between the Mn_1 atoms, and it is much stronger than the interaction between the Mn_1-Mn_2 and Mn_2-Mn_2 atoms [16]. In contrast, the interaction (J_3) between the nearest neighbors Mn_2-Mn_2 strongly depends on the related atomic distance (d_3). The neighboring Mn_2 atoms are ferromagnetically (FM) coupled in the fully relaxed unit cell where $d_3 = 3.017$ Å [based on density-functional theory (DFT) calculation]. By applying compressive strain, d_3 decreases and the corresponding FM

*y.xie@hzdr.de
†s.prucnal@hzdr.de

coupling is suppressed, then transformed into antiferromagnetic (AFM) coupling. In theoretical calculations presented by Slipukhina *et al.* [16], when $d_3 = 2.974$ Å, the neighbor Mn_2 atoms are AFM coupled. The competing interactions between the AFM coupling between Mn_2 and the FM coupling between Mn_1 atoms stabilize noncollinear spin configurations [17,18]. The transition temperature from collinear to noncollinear magnetism in Mn_5Ge_3 is 70 ± 5 K [19,20] which is usually explained by similar lattice distortions observed in Mn_5Si_3 [21–23]. Yet there is no convincing explanation why the noncollinear spin configuration appears in nanostructured Mn_5Ge_3 but not in bulk materials [16,19,20].

To gain insight into the complex physical properties of ferromagnetic Mn_5Ge_3 thin films, we have performed systematically experimental investigation using temperature and angular-dependent magnetoresistance, temperature-dependent x-ray diffraction (TDXRD) as well as theoretical calculations using DFT [24–26]. According to our theoretical calculations the exchange constant J_3 becomes negative and the nearest-neighboring Mn_2-Mn_2 atoms are AFM coupled for a $d^{\mathrm{DFT}}{}_3$-value on the order of 3.002 Å or smaller. The relative distance $d^{\mathrm{exp}}{}_3$ between two neighbor Mn_2 atoms, extracted experimentally from TDXRD, shrinks from 3.012 ± 0.002 Å at room temperature down to 2.999 ± 0.002 Å at 5 K. The critical distance for the neighboring Mn_2 atoms (d_3 smaller than 3.002 Å) at which magnetic coupling changes from FM to AFM is achieved at the temperature of 150 ± 10 K. This means that at low temperatures the AFM coupling of Mn_2 atoms coexists with FM coupling of Mn_1 atoms. At higher temperatures, all coupling interaction between Mn atoms is ferromagnetic. The temperature-dependent anisotropic magnetoresistance (AMR) reveals a well-visible transition from twofold to multifold symmetry with increasing temperature. This work provides experimental and theoretical evidence that both the switching between noncollinear and collinear spin configurations and the intriguing behavior of AMR are caused by the change of the magnetic coupling between Mn_2 atoms occupying 6g positions in the Mn_5Ge_3 sublattice.

II. RESULTS AND DISCUSSION

A. Magnetotransport results

In this work, (100)-orientated Mn_5Ge_3 epitaxial films were fabricated on (001) Ge substrates by ms-range solid-state reaction (see the inset in Fig. 1) [3]. Figure 1 shows the temperature-dependent resistivity ($\rho - T$) and the related first derivative curve of the Mn_5Ge_3 thin film. In the $d\rho/dT$ curve, a clear transition from positive to negative near 283 K is observed, which mainly ascribed to the transition from ferromagnetic to paramagnetic state [3,6,7,27]. The observed T_C corresponds well to the value obtained by superconducting quantum interference device–vibrating-sample magnetometer measurements (see Fig. S1 in Supplemental Material [28]). Below T_C (283 K) the resistivity decreases with decreasing temperature, showing typical metallic behavior [16,29,30]. Below T_C, the carrier-magnon scattering must be taken into account as well since the electron-magnon scattering dominates the electrical transport properties in strong ferromagnetic films.

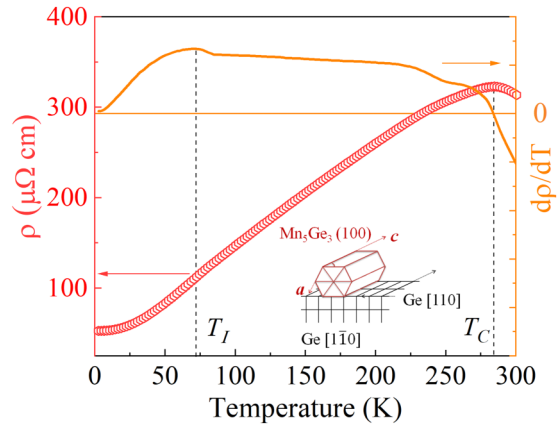

FIG. 1. Temperature dependence of the resistivity for a (100)-oriented Mn_5Ge_3 film grown on Ge (001) substrate (red circles) and the corresponding first derivative (yellow curve). The inset shows the schematic alignment of the Mn_5Ge_3 and Ge unit cells where the hexagonal Mn_5Ge_3 (100) is twisted with respect to the ⟨110⟩ of cubic Ge (001). Here, we only show one case where the c axis of Mn_5Ge_3 is roughly oriented along the [110] direction of Ge.

It is worth noting there is another small deformation (kind of cusp) in the $d\rho/dT$ curve at $T_I \sim 72$ K beside the well-visible transition at T_C. Such a cusp is commonly observed in Mn_5Ge_3 thin films and nanostructures but has not been shown in bulk crystals [19,20,31]. The appearance of such a cusp in the $d\rho/dT$ curve is often related to the emergence of a new magnetic ordering. Zeng *et al.* reported that the cusp is due to the coexistence of two magnetic sublattices (Mn_1 and Mn_2) with different magnetocrystalline anisotropies and exchange coupling constants [19]. The change of the magnetic coupling between Mn atoms was concluded by an analogy to the antiferromagnetic Mn_5Si_3 where noncollinear spin states exist at lower temperatures [21,23,32]. The nontrivial spin arrangements at lower temperatures were demonstrated to induce the topological Hall effect [23,33]. To date, no further interpretation has been proposed to understand the underlying mechanism why the noncollinear spin configuration exists in Mn_5Ge_3 films.

The AMR is a response of the electronic structure in magnetic materials to the variation of the magnetization direction. In traditional AMR theory of ferromagnetic metals [34,35], the magnetoresistance exhibits maximum value when the current is parallel to the magnetization direction, in which carriers moving along the magnetized direction are experiencing the strongest scattering potential among all Fermi surface states, whereas it shows a minimum when the current flow is perpendicular to the magnetization direction. This theory is valid for polycrystalline and amorphous ferromagnets in which the AMR only depends on the relative orientation of magnetization and current. However, in the case of epitaxial or strongly textured crystalline ferromagnetic films, such as Mn_5Ge_3 grown on Ge, the AMR depends also on the orientation of magnetization with respect to the crystalline axes. The AMR can be decomposed into two parts, noncrystalline and crystalline terms [28,36–39]. For the noncrystalline component the AMR depends on the angle between the cur-

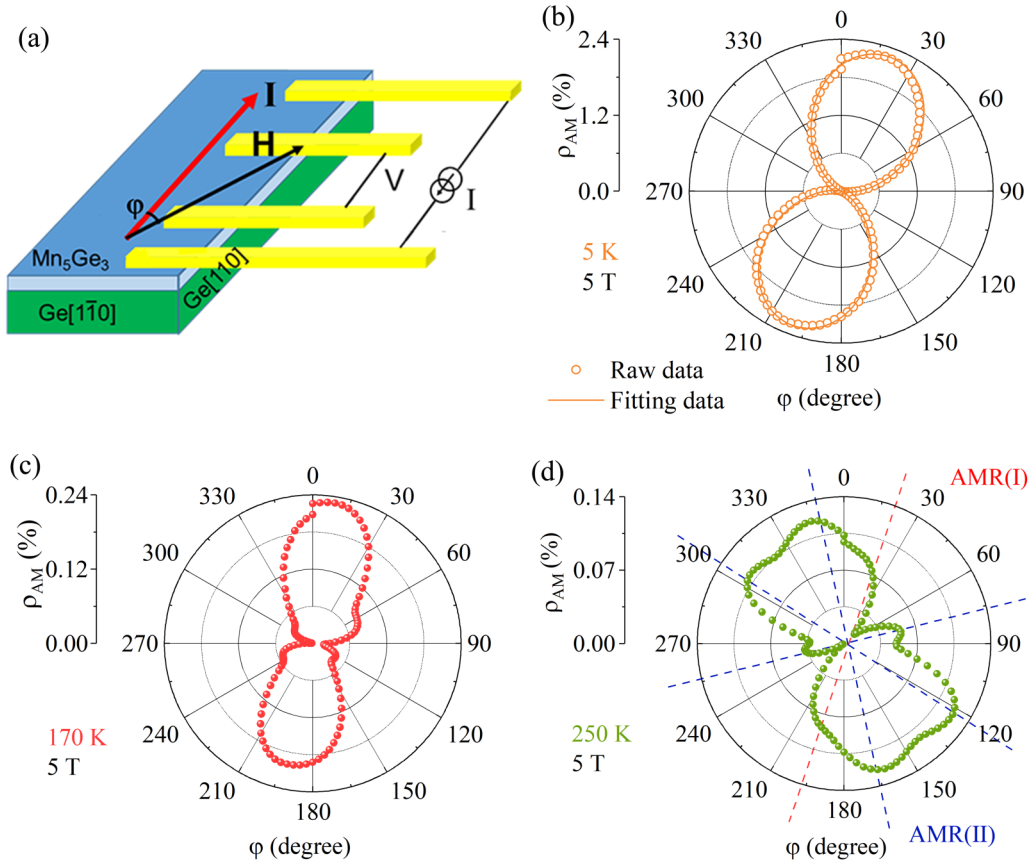

FIG. 2. (a) Schematic representation of the angular-dependent magnetoresistance measurements geometry. The electric current I flows parallel to the [110] direction of Ge and the magnetic field was rotated in the surface plane (001) of Ge. The angular-dependent magnetoresistance ρ_{AM} with in-plane magnetic field of 5 T as a function of the angle (φ) between magnetic field and current were measured at (b) 5 K, (c) 170 K, and (d) 250 K. ρ_{AM} is defined as $[(\rho(\varphi) - \rho_{min})/\rho_{min}] \times 100\%$.

rent and magnetization, but is independent of the orientation of magnetization with respect to the crystalline axes. On the other hand, the crystalline component relies on the symmetry of the crystal structure and is independent of the current direction.

Magnetotransport measurements were performed using four-wire contacts designed in a row [see Fig. 2(a)]. Figures 2(b)–2(d) show the angle (φ)-dependent anisotropic magnetoresistance ρ_{AM} measured at various temperatures with magnetic field applied in-plane sample surface. As shown in Fig. S2, the AMR maxima and minima of (100)-oriented Mn_5Ge_3 are almost independent of the current flow direction but strongly dependent on the crystalline axis, which indicates dominating crystalline AMR. Therefore, the observed evolution of anisotropy in magnetoresistance can be tentatively attributed to the crystalline component of the AMR. The magnitude of the ρ_{AM} and its dependence on φ are quite diverse with temperature rising from 5 to 300 K. At 5 K [see Fig. 2(b)], ρ_{AM} has a large modulation (2.24%) as a function of φ that accurately follows a typical $\cos^2\varphi$ dependence. It exhibits twofold symmetry [AMR(I)] with global minimum values at about 110° and 290° while global maximum values are observed at about 20° and 200°. The current is injected along the [110] lattice plane of Ge while the AMR response at 5 K is originated from the ferromagnetic Mn_5Ge_3 layer. As shown in the inset of Fig. 1, the out-of-plane $[210]_H$ direction of Mn_5Ge_3 is parallel to the $[001]_C$ direction of Ge substrate (the subscript indexes H and C denote the hexagonal and cubic unit cells, respectively) [3]. The $[001]_H$ direction of Mn_5Ge_3 lies in the surface plane of the Ge (001) substrate, and is roughly oriented along the $\langle 110\rangle_C$ direction of Ge. Due to the relatively large lattice mismatch between Mn_5Ge_3 and Ge the unit cell of the ferromagnetic film is misoriented in all directions, resulting in the tilt of the (100) net planes and a twist in the basal plane. The tilt/rotation of the Mn_5Ge_3 layer with respect to the Ge substrate is likely related to the shift of the twofold symmetry global maximum in the AMR signal with respect to the injected current, consistent with our finding of dominating crystalline AMR. The AMR symmetry changes with increasing temperature. Most probably, this is mainly due to the change of the magnetic coupling between Mn_2 atoms with increasing interatomic distance between them. The twofold AMR contributed from Mn_1 atoms becomes weaker while the additional AMR component with new symmetries contributed from Mn_2 becomes stronger with increasing temperature. With increasing temperature, the Mn_2 atoms in the 6g site become FM coupled, which changes the distribution of the local magnetic moments and results in a multifold symmetry in the AMR signal [schematically marked with blue dashed lines in Fig. 2(d)]. At this temperature, the multifold symmetry coexists with the Mn_1-related twofold symmetry as schematically shown in Fig. 2(d).

Now we discuss the AMR evolution in detail. Firstly, with increasing temperature from 5 to 150 K, the magnitude of ρ_{AM} reduces from 2.24 to 0.38%, but still shows the identical twofold AMR [Figs. S3(a)–S3(c)] [28]. At 170 K [see Fig. 2(c)], besides the AMR(I) component with twofold symmetry, additional local peaks emerge along several specific angular directions (i.e., $\varphi = 70°$, 115°, 160°, 250°, 295°, and 340°). At 250 K [see Fig. 2(d)], the magnitude of inherent twofold AMR(I) is strongly suppressed (reduced to 0.07%), while the newly emerged AMR(II) component becomes stronger and new global maxima appear at $\varphi = 75°$, 125°, 175°, 255°, 305°, and 355°. At 250 K the AMR(II) increases up to 0.12% for the global maximum at 125°. With increasing temperature from 170 to 250 K the angle interval between maxima in AMR(II) changes from 45° to 50°. The position of the global maximum changes with increasing temperature. Most probably, the rotation of the global maximum is due to the structural deformation of the Mn_5Ge_3 unit cell with temperature causing a change in the spatial position of the Mn atoms. At 300 K, the Mn_5Ge_3 is paramagnetic and the related ρ_{AM} curve exhibits a twofold symmetry again (see Fig. S4) [28].

To explain the transition of spin configurations at 72 K and the diverse AMR symmetries observed at different temperature regimes, the magnetotransport properties of Mn_5Ge_3 are further discussed in terms of structural evolutions and corresponding DFT calculations.

B. Structural analysis

Figures 3(a) and 3(b) show the distances d_3 and d_1 between the nearest-neighboring atoms in Mn_2 and Mn_1 sublattices extracted from the TDXRD results (see Fig. S5) [28,40,41], respectively. Upon cooling, both d_3 and d_1 distinctly shrink with decreasing the temperature. At 150 K, d_3 reduces to 3.002 Å. Here, for the calculation of d_3 we assumed an identical change of the d_3 for all Mn_2 atoms in the basal configuration and a constant parameter of the 6g Wyckoff position. In fact, while the basal configuration of the Mn_2 unit in relaxed Mn_5Ge_3 is an equilateral triangle, only one side is aligned along the out-of-plane direction in our film geometry. Nevertheless, the assumptions made here are sufficient to present qualitatively the influence of the temperature-dependent strain and the unit-cell deformation on the AMR and spin configuration. It is important to note that the decreasing of d_3 is much faster than d_1. This is due to the different thermal expansion coefficient (α) for the semimetallic Mn_5Ge_3 film (the average $\alpha = 2.6 \times 10^{-5}\,K^{-1}$) and for semiconducting Ge ($\alpha = 6.1 \times 10^{-6}\,K^{-1}$) [8]. For the Mn_5Ge_3 film, the change of the out-of-plane lattice parameter is about four times larger than the change of the in-plane lattice parameter that depends on the Ge substrate. As a result, the hexagonal unit cell is flattened and distorted at lower temperatures, where the Mn_5Ge_3 unit cell has the large *c*/*a* ratio.

C. Density-functional theory (DFT) calculations

To understand the roles of accumulated strains on the magnetotransport properties of experimental samples, we carried out the computations [42–46] assuming the relative change

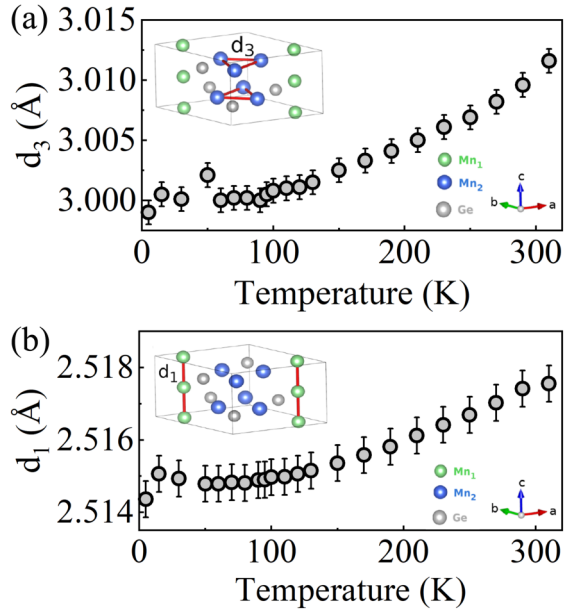

FIG. 3. (a), (b) Temperature-dependent distances d_3 and d_1 between the nearest-neighbor atoms in Mn_2 and Mn_1 sublattices as deduced from TDXRD and tabulated lattice spacing at room temperature ($d_3^0 = 3.017$ Å, $d_1^0 = 2.518$ Å) [14], respectively. Error bars are shown for the measured atomic distances d_3 and d_1 while the error in the temperature is within the size of the used data symbols. The insets in (a) and (b) show the schematic picture of the crystal structure. The Mn_1, Mn_2, and Ge atoms are shown with green, blue, and gray circles, respectively.

of the lattice values obtained from the experiments. In order to gain insight into macroscopic magnetism revealed in the experimental samples, it is crucial to examine the microscopic picture. Note that the macroscopic magnetism originates from short-range exchange couplings that constitute the microscopic magnetic model. Moreover, any microscopic magnetic model is apparently related to the geometrical features of the underlying crystal structure, in particular, the mutual arrangements of the magnetic atoms. Thus, it is crucial to consider the distances between the nearest-neighboring Mn ions in each of two sublattices for the magnetic ground state (M_1 configuration in Fig. S6) [28]. Mn_5Ge_3 films invariably present ferromagnetic behavior with the exertion of experimental strain, in accordance with previously reported results [15,16].

Furthermore, we examine the impact of the elastic strains on the exchange interactions between the Mn spins (shown in Fig. 4), by considering an effective classical spin Hamiltonian [46]. The details of these calculations along with derived equations are presented in Supplemental Material [28] (see Figs. S6–S8).

Note that the nearest-neighbor interaction between the Mn_1-Mn_1 exhibits FM exchange coupling J_1, which dominates over the remaining interactions. See Table I. The negligible changes in J_1 are reflected by the very small changes of d_1 distances, which are approximately 0.003 Å between 300 and 5 K. In the case of the Mn_2 sublattice the AFM coupling appears under the compressive strain. The AFM interaction is more favorable for the Mn_2 sublattice when the d_3 distance is getting shortened, in agreement with

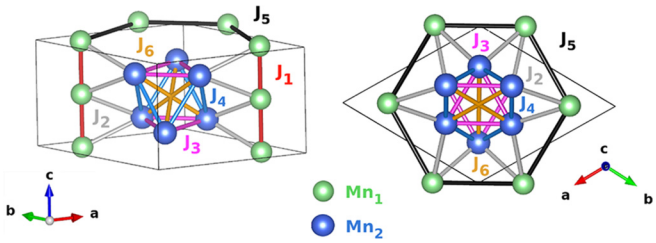

FIG. 4. Schematic picture of the crystal structure and exchange couplings. Different colors indicate various Mn-Mn distances and the corresponding exchange couplings. The thin black lines denote the size of the unit cell. The Mn_1 and Mn_2 atoms in the sublattices with fourfold and sixfold positions are marked with green and blue color. The Ge atoms are not shown here and the unit cell is shifted to (0.5, 0.5, 0).

previously reported calculations [16]. However, note that in Ref. [16] the authors reported a larger change of J_3 [from −2.04 (rigid) to 1.80 meV (relaxed)] which corresponds to a larger shortening of the d_3 distance (0.083 Å presented in Ref. [16] vs 0.017 Å obtained in this work). The latter is probably a consequence of different and larger strain used in comparison to our simulations, not directly stated in Ref. [16]. According to our DFT calculation, for d_3 larger than 3.002 Å the Mn_2 sublattice exhibits ferromagnetism. However, the Mn atoms in the Mn_2 sublattice are AFM coupled for the d_3 smaller than 3.002 Å.

D. Discussion

Finally, we propose a scenario for the noncollinear to collinear switching and anomalous AMR behavior as a function of temperature. During the cooling process, d_3 becomes smaller than 3.002 Å at a temperature below 150 K (see Fig. 3). Furthermore, the FM coexists with AFM states at low temperatures in Mn_5Ge_3 films. Since the AFM coupling in the Mn_2 sublattice induces the change of local spin ordering, it would exert different influence on the AMR. In addition, it has been reported that the electronic properties of Mn_5Ge_3 depend strongly on the atomic distance and atomic environment of Mn atoms [28]. In this case, the magnetoresistance below 150 K with a twofold symmetry can be related to the interaction between conduction electrons and FM spin ordering in the Mn_1 sublattice. In the temperature range from 150 to 280 K the AMR shows combination of both twofold and multifold symmetry. We infer that the twofold symmetry is caused by FM coupling between Mn atoms with fourfold position in the Mn_1 sublattice. The multifold symmetry is probably associated with the FM coupling between Mn_2 atoms with sixfold position in the Mn_2 sublattice.

In addition, the coexistence of AFM and FM coupling observed at low temperatures probably contributes to a low-temperatures noncollinear spin configuration which is commonly observed in Mn_5Ge_3 thin films. With temperature decreasing below 150 K, the AFM coupling between Mn_2 atoms is increasing. So, the magnetic state depends on the distance between the Mn atoms, and spins will rotate to adjust to the new positions of the atoms with temperature decreasing. Upon cooling to 70 K, the strong enough AFM coupling can compete with FM coupling, and thus it is highly plausible to result in the noncollinear spin state. Moreover, Stroppa and Peressi have shown that the noncollinear spin configuration in Mn_5Ge_3 is stabilized at a higher c/a ratio [15]. In our work, Mn_5Ge_3 exhibits a larger c/a ratio with decreasing temperature, which additionally justifies the existence of noncollinear spin configuration below 70 K. The experimental error in the presented atomic distances might also contribute to the discrepancy between these two identified characteristic temperatures.

TABLE I. Exchange couplings for the strained Mn_5Ge_3 samples at 5 K and unstrained Mn_5Ge_3. Negative and positive J_{ij} values denote AFM and FM couplings, respectively. The changes in distances are given in respect to the FM ground state.

$J_{ij}(d_{ij})$ (meV)	Strained at 5 K	Unstrained
$J_1^{\text{Mn1-Mn1}}(\Delta d_1)$	33.2 (0.003 Å)	33.6
$J_2^{\text{Mn1-Mn2}}$	6.9	8.4
$J_3^{\text{Mn2-Mn2}}(\Delta d_3)$	−0.2 (0.017 Å)	1.0
$J_4^{\text{Mn2-Mn2}}$	5.7	5.7
$J_5^{\text{Mn1-Mn1}}$	8.2	8.5
$J_6^{\text{Mn2-Mn2}}$	4.8	4.8

III. CONCLUSION

In summary, the ferromagnetic Mn_5Ge_3 films grown on Ge substrates show anomalous temperature-dependent AMR and switching from noncollinear to collinear spin configuration. Using different experimental techniques combined with DFT calculations, we have proposed a physical scenario responsible for both anomalous AMR and the switch of the spin configuration. The low-temperature noncollinear spin configuration very probably arises from the coexistence of AFM and FM coupling between Mn atoms in the Mn_2 and Mn_1 sublattices. The change of the magnetic coupling between Mn atoms in the Mn_2 sublattice from AFM to FM is proposed as an explanation for the anomalous AMR behavior as a function of temperature. Our results would stimulate further investigations to understand the intriguing magnetic properties in Mn_5Ge_3 films.

ACKNOWLEDGMENTS

Y.X. (File No. 201706340054) acknowledges the financial support by China Scholarship Council. M.B. is funded by the National Science Centre Grant No. UMO-2016/23/D/ST3/03446. Access to computing facilities of PL-Grid Polish Infrastructure for Supporting Computational Science in the European Research Space and of the Interdisciplinary Center of Modeling (ICM), University of Warsaw is gratefully acknowledged. We made use of computing facilities of TU Dresden ZIH within the project "TransPheMat." The low-temperature x-ray diffraction was performed in MGML [47], which was supported within the program of Czech Research Infrastructures (Project No. LM2018096).

Author Y.X. performed the basic magnetic and transport measurements. Y.Y. and C.Z. performed angular-dependent

magnetoresistance measurements. P.D. and D.K. performed the temperature-dependent XRD measurements. M.B. performed the DFT calculations and related analyses. J.G. contributed to the discussion about structural analyses. D.K. and X.Z. contributed to the discussion about transport analyses. M.H., S.Z., L.C., Y.-J.Z., and M.W. contributed to the revision of the manuscript. S.P. designed and supervised the whole project.

[1] I. Žutić, J. Fabian, and S. D. Sarma, Rev. Mod. Phys. **76**, 323 (2004).
[2] X. Jiang, R. Wang, R. M. Shelby, R. M. Macfarlane, S. R. Bank, J. S. Harris, and S. S. P. Parkin, Phys. Rev. Lett. **94**, 056601 (2005).
[3] Y. Xie, Y. Yuan, M. Wang, C. Xu, R. Hübner, J. Grenzer, Y. J. Zeng, M. Helm, S. Zhou, and S. Prucnal, Appl. Phys. Lett. **113**, 222401 (2018).
[4] Y. S. Dedkov, M. Holder, G. Mayer, M. Fonin, and A. B. Preobrajenski, J. Appl. Phys. **105**, 073909 (2009).
[5] W. Ndiaye, J.-M. Mariot, P. De Padova, M. C. Richter, W. Wang, O. Heckmann, A. Taleb-Ibrahimi, P. Le Fèvre, F. Bertran, C. Cacho, M. Leandersson, T. Balasubramanian, A. Stroppa, S. Picozzi, and K. Hricovini, Phys. Rev. B **91**, 125118 (2015).
[6] A. Spiesser, F. Virot, L. A. Michez, R. Hayn, S. Bertaina, L. Favre, M. Petit, and V. LeThanh, Phys. Rev. B **86**, 035211 (2012).
[7] V. LeThanh, A. Spiesser, M. T. Dau, S. F. Olive-Mendez, L. A. Michez, and M. Petit, Adv. Nat. Sci. Nanosci. **4**, 043002 (2013).
[8] D. D. Dung, D. Odkhuu, L. Thanh Vinh, S. Cheol Hong, and S. Cho, J. Appl. Phys. **114**, 073906 (2013).
[9] T. Nie, J. Tang, X. Kou, Y. Gen, S. Lee, X. Zhu, Q. He, L. T. Chang, K. Murata, Y. Fan, and K. L. Wang, Nat. Commun. **7**, 12866 (2016).
[10] M. Gajdzik, C. Sürgers, M. Kelemen, H. V. Löhneysen, and M. Materials, J. Magn. Magn. Mater. **221**, 248 (2000).
[11] A. Spiesser, I. Slipukhina, M. T. Dau, E. Arras, V. Le Thanh, L. Michez, P. Pochet, H. Saito, S. Yuasa, M. Jamet, and J. Derrien, Phys. Rev. B **84**, 165203 (2011).
[12] R. F. Jackson, R. G. Scurlock, D. B. Utton, and E. M. Wray, Proc. Phys. Soc. **85**, 127 (1965).
[13] G. Kappel, G. Fischer, and A. Jaegle, Phys. Status Solidi A **34**, 691 (1976).
[14] J. Forsyth and P. J. Brown, J. Condens. Matter Phys. **2**, 2713 (1990).
[15] A. Stroppa and M. Peressi, Phys. Status Solidi A **204**, 44 (2007).
[16] I. Slipukhina, E. Arras, P. Mavropoulos, and P. Pochet, Appl. Phys. Lett. **94**, 192505 (2009).
[17] J. M. D. Coey, Can. J. Phys. **65**, 1210 (1987).
[18] Y. O. Kvashnin, W. Sun, I. Di Marco, and O. Eriksson, Phys. Rev. B **92**, 134422 (2015).
[19] C. Zeng, S. C. Erwin, L. C. Feldman, A. P. Li, R. Jin, Y. Song, J. R. Thompson, and H. H. Weitering, Appl. Phys. Lett. **83**, 5002 (2003); C. Zeng, Y. Yao, Q. Niu, and H. H. Weitering, Phys. Rev. Lett. **96**, 037204 (2006).
[20] J. Tang, C. Y. Wang, W. Jiang, L. T. Chang, Y. Fan, M. Chan, C. Wu, M. H. Hung, P. H. Liu, H. J. Yang, and H. Y. Tuan, Nano Lett. **12**, 6372 (2012).
[21] P. J. Brown, J. B. Forsyth, V. Nunez, and F. Tasset, J. Condens. Matter Phys. **4**, 10025 (1992); P. J. Brown and J. B. Forsyth, *ibid.* **7**, 7619 (1995).
[22] J. Leciejewicz, B. Penc, A. Szytuła, A. Jezierski, and A. Zygmunt, Acta Phys. Pol. A **113**, 1193 (2008).
[23] C. Surgers, G. Fischer, P. Winkel, and H. V. Löhneysen, Nat. Commun. **5**, 3400 (2014).
[24] P. Hohenberg and W. Kohn, Phys. Rev. **136**, B864 (1964).
[25] W. Kohn and L. J. Sham, Phys. Rev. **140**, A1133 (1965).
[26] J. P. Perdew, K. Burke, and M. Ernzerhof, Phys. Rev. Lett. **77**, 3865 (1996).
[27] S. Bechler, M. Kern, H. S. Funk, G. Colston, I. A. Fischer, D. Weißhaupt, M. Myronov, J. Van Slageren, and J. Schulze, Semicond. Sci. Technol. **33**, 095008 (2018).
[28] See Supplemental Material at http://link.aps.org/supplemental/10.1103/PhysRevB.104.064416 for the discussion of temperature-dependent magnetization, the AMR measurement details and more AMR results and discussion, TDXRD measurement details and analysis of the related raw data, theoretical calculations, and additional results.
[29] C. Sürgers, G. Fischer, P. Winkel, and H. V. Löhneysen, Phys. Rev. B **90**, 104421 (2014).
[30] S. Picozzi, A. Continenza, and A. J. Freeman, Phys. Rev. B **70**, 235205 (2004).
[31] N. Yamada, J. Phys. Soc. **59**, 273 (1990).
[32] A. Z. Menshikov, A. P. Vokhmyanin, and Y. A. Dorofeev, Phys. Status Solidi B **158**, 319 (1990).
[33] H. Reichlová *et al.*, arXiv:2012.15651.
[34] J. Smit, Physica **17**, 612 (1951).
[35] T. McGuire and R. L. Potter, IEEE Trans. Magn. **11**, 1018 (1975).
[36] W. Döring, Ann. Phys. **424**, 259 (1938).
[37] B. Howells, M. Wang, K. Edmonds, P. Wadley, R. Campion, A. Rushforth, C. Foxon, and B. L. Gallagher, Appl. Phys. Lett. **102**, 052407 (2013).
[38] R. P. van Gorkom, J. Caro, T. M. Klapwijk, and S. Radelaar, Phys. Rev. B **63**, 134432 (2001).
[39] Y. Yuan, R. Hübner, M. Birowska, C. Xu, M. Wang, S. Prucnal, R. Jakiela, K. Potzger, R. Böttger, S. Facsko, J. A. Majewski, M. Helm, M. Sawicki, S. Zhou, and T. Dietl, Phys. Rev. Materials **2**, 114601 (2018).
[40] M. S. Henriques, D. I. Gorbunov, D. Kriegner, A. V. A. M. Vališka, and Z. Matěj, J. Magn. Magn. Mater. **400**, 125 (2016).
[41] D. Kriegner, Z. Matěj, R. Kužel, and V. Holý, J. Appl. Crystallogr. **48**, 613 (2015).
[42] G. Kresse and J. Hafner, Phys. Rev. B **47**, 558 (1993).
[43] G. Kresse and J. F. Mueller, Comput. Mater. Sci. **6**, 15 (1996).
[44] P. E. Blochl, Phys. Rev. B **50**, 17953 (1994).
[45] G. Kresse and D. Joubert, Phys. Rev. B **59**, 1758 (1999).
[46] S. L. Dudarev, G. A. Botton, S. Y. Savrasov, C. J. Humphreys, and A. P. Sutton, Phys. Rev. B **57**, 1505 (1998).
[47] http://mgml.eu/.